Tampere University

Iuliia Dmitrieva

ER-DOPED GLASS-CERAMICS

Faculty of Natural Sciences
Bachelor of Science Thesis
November 2019

ABSTRACT

Iuliia Dmitrieva: Er-doped glass-ceramics
Bachelor of Science Thesis
Tampere University
Bachelor's Degree Program in Science and Engineering
November 2019

This study was focused on investigation of new glass-system with the following composition: (100-x-0.25)(75$NaPO_3$ – 25CaF_2) – xFe_2O_3 – 0.25Er_2O_3 with x = 0, 1.5, 2.5, 5, and 10 in mol%. The new system is contrasting with the previous studies due to the integration of Fe_2O_3 into the composition. The aim of the study was to improve the thermal stability of the glass while ensuring the preservation of the nucleation and growth mechanisms.

Glasses were prepared using a standard melting process and characterized, after which the glass-ceramics were made by controlled heat treatment of the as-prepared glasses. The results demonstrate improved thermal stability, but along with loss in fluorine content during melting, which prevented CaF_2-crystals formation in glass-ceramics. The use of quartz crucible induces a change in fluorine content and, as a consequence, the nucleation and growth mechanisms.

Keywords: phosphate glass, laser glass, rare earth, glass-ceramics, nucleation and growth

PREFACE

This study was made in the scope of a Bachelor's Thesis project as a part of study programme in Science and Engineering, BSc int. at Tampere University. The experimental investigation was conducted in the Photonics Laboratory, Faculty of Engineering and Natural Sciences, as a part of the Photonic Glasses research group under the supervision of Associate Professor Laeticia Petit.

I would like to thank Laeticia Petit for the guidance and support throughout my research process. Furthermore, I would like to thank all people in the Photonic Glasses research group for help with the experiments and equipment.

Tampere, 20th November 2019

Iuliia Dmitrieva

CONTENTS

LIST OF FIGURES

LIST OF SYMBOLS AND ABBREVIATIONS

A	absorbance
I	intensity
L	thickness of glass sample
m	mass
N	ion concentration
T	temperature
ΔT	temperature difference
α	absorption coefficient
λ	wavelength
ρ	density
σ	absorption cross-section

°C	degrees Celsius (0 °C = 273.15K) g gram (1 g = 10^{-3} kg)
cm	centimeter (1 cm = 10^{-2} m)
μm	micrometer (1 μm = 10^{-6} m)
nm	nanometer (1 nm = 10^{-9} m) s second
min	minute (1 min = 60 s)
h	hour (1 h = 60 min)

A.U.	Arbitrary Unit
ATR	Attenuated Total Reflection
DTA	Differential Thermal Analysis
DSC	Differential Scanning Calorimetry
FTIR	Fourier Transform Infrared Spectroscopy
GCs	glass-ceramics
HT	heat treatment
IR	infrared
RE	rare earth
SEM	Scanning Electron Microscopy
T_m	glass melting temperature
T_g	glass transition temperature
T_x	glass crystallization temperature
T_p	glass crystallization peak temperature
XRD	X-Ray Diffraction

CaF_2	calcium fluoride
Fe_2O_3	iron(III) oxide
Er_2O_3	erbium(III) oxide
Er^{3+}	trivalent erbium ion
$NaPO_3$	sodium(I) metaphosphate
$(NaPO_3)_6$	sodium(I) hexametaphosphate
Pt	platinum

1. INTRODUCTION

“Photonics is a systematic science dealing with the photon generation and detection, as well as stimulated emission, photon frequency conversion and polarization change. (Xu,06)” Glass has a potential to become a photonic medium since it can be doped with rare-earth (RE) elements and nanoparticles, and many other properties can be altered to fit various applications.

Phosphate glasses have been of a great interest because they can be designed to possess good solubility of rare-earth ions without clustering effect and also good thermal and mechanical stabilities along with low melting temperature and other (Sh,05). Glasses containing RE-ions possess distinctive spectroscopic properties and due to that have a number of different applications, such as lasers, telecommunications area, optical amplifiers, solar cells, bio-imaging and other (De,98).

This thesis is the continuation of the study of Er-doped glasses and glass-ceramics (No,18), (Sz,19). Er^{3+} doped glasses with the composition (75 $NaPO_3$-(25-x) CaO-xCaF_2) (in mol %) were prepared using standard melting process and characterized. The newly developed glasses were found to be promising materials for upconversion applications, especially the glass with x=25. This glass exhibits a bulk crystallization upon heat treatment with the precipitation of CaF_2 crystals. Due to a significant increase in the intensity of the upconversion, the CaF_2 crystals are expected to contain Er^{3+} ions. However, the glass exhibits a poor thermal stability limiting its drawing into fiber. In this work, different amounts of Fe_2O_3 were added into the glass with x=25 in order to create a more thermally stable glass. The glasses were heat treated to check the impact of the Fe addition on the crystallization tendency of the glass. Therefore, the objective of this work was to study the impact of Fe_2O_3 addition on various glass properties and on the nucleation and crystallization mechanism.

In Chapter 2, the basic definitions of glass, laser glass, glass-ceramics are introduced. Fundamental concepts such as glass formation, glass melting, nucleation and growth theory are presented. Next, Chapter 3 focuses on the experimental part of the study; preparation of the samples and operation principles of all equipment used for glass characterization are described. The results and analysis of the measurements follow in Chapter 4, along with a discussion based on the objectives and acquired data. Chapter 5 concludes the study, proposing the next step.

2. THEORETICAL BACKGROUND

2.1 Glasses

Glass is a material that is usually characterized by the following properties: hard, inorganic, transparent, and brittle substance. History of glass counts centuries of glass manufacturing, the earliest glass objects are dated as early as 2500 BCE produced in Egypt (Gl,19). Glass manufacturing employs various techniques for different applications, which includes both practical and decorative utilization such as building construction, housewares, and telecommunications (Gl,19).

2.1.1 Glass formation

To comprehend the nature of glass and its formation mechanism, the glass formation process can be studied by reviewing one of the most prominent diagrams in glass science, enthalpy versus temperature plot (Figure 1).

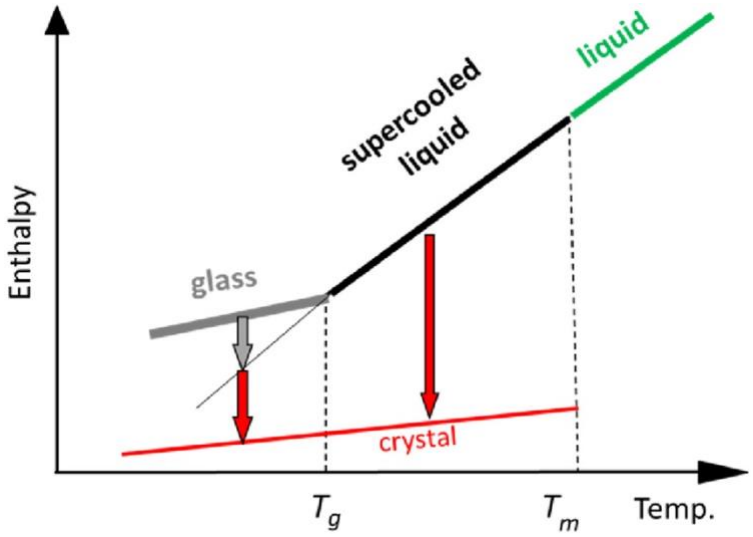

Figure 1. *Enthalpy versus temperature plot for the glass formation mechanism (Za,17).*

Different stages of the material can be defined as:

- Liquids, which exist above the melting temperature T_m and never crystalizes
- Supercooled liquids, which exist between T_m and the glass transition temperature T_g, they crystalize eventually (as indicated by the red arrow);
- Glasses, which exist below the T_g, they spontaneously relax toward the supercooled liquids at any nonzero temperature as indicated by the gray arrow and eventually crystalize;
- Crystals, which possess well-organized atomic structures at short, medium and long range and are stable below the T_m (Za,17).

Therefore, the glass formation mechanism can be described as following: the liquid melt is cooled down and the molecular motion slows down, reaching T_m it can crystalize or in

case of rapid cooling transform into supercooled liquid (no crystalline structure is formed), during cooling. The growing viscosity of the material does not allow the atomic structure to completely rearrange to an ordered crystalline structure. Finally, when the temperature reaches T_g, an amorphous material called glass is formed. 'Amorphous' indicates no long-order range or periodic atomic arrangement.

2.1.2 Glass definition

The complete definition of glass based on its formation process is: "Glass is a nonequilibrium, non-crystalline condensed state of matter that exhibits a glass transition. The structure of glasses is similar to that of their parent supercooled liquids, and they spontaneously relax toward the supercooled liquids state. Their ultimate fate, in the limit of infinite time, is to crystallize." (Za,17)

Glasses are also described by their various properties: optical properties, such as index of refraction, light absorption/transmission; mechanical properties, such as viscosity, density, compression resistance; thermal properties, such as thermal expansion coefficient, glass characteristic temperatures. All the properties are defined by the chemical composition of a particular glass.

2.1.3 Glass melting

Glass manufacturing process can be described in terms of distinct basic steps: preparation of a batch from raw materials (chemicals), heat-melting of the batch in the melting furnace and enforcing cooling of the newly formed glass by quenching. The next and final crucial step is annealing of the newly formed glass to diminish the stress after the quenching and produce a stable glass.

Indeed, glasses may be manufactured in many different ways and utilizing different chemical composition, however, the most prevalent glass manufacturing technique is melting silica (SiO_2) with other oxides, often referred to as soda-lime-silica glasses. To prepare such a glass, silica (SiO_2) is mixed with soda (Na_2O) in the form of sodium carbonate to lower the melting temperature, then the lime (CaO) in the form of calcium carbonate is added to increase the chemical durability of the glass. (We,19)

Sol-gel is another widely used technique, which encompasses the formation of polymeric sols originating at hydrolysis and condensation of the precursors. Then, as hydrolysis and condensation advances, the gels are formed. (Kh,15)

2.2 Optical glasses

2.2.1 Phosphate glasses

Phosphate glasses are one of the alternative glasses, which are based on phosphorus pentoxide (P_2O_5) tetrahedral units (Figure 2). The P-tetrahedra derive from the formation

of sp_3 hybrid orbitals by the P outer electrons ($3s_2 3p_3$) and the outer electron is promoted to a 3d orbital where 3d orbital forms strong π-bonding molecular orbitals with oxygen 2p electrons. These tetrahedral units associate through covalent bridging oxygens to build various phosphate anions. Phosphate tetrahedral units in phosphate glasses are classified using Q_i terminology (Figure 2), where *i* stands for the number of bridging oxygens per tetrahedron. (Br,00)

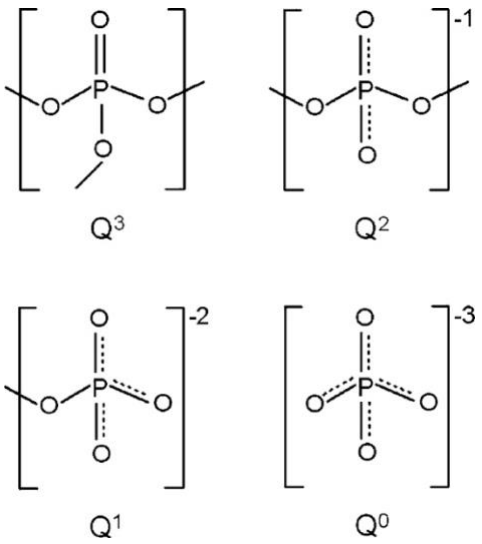

Figure 2. *Schematic representation of Q_i phosphate tetrahedral units in phosphate glasses (Ko,10).*

Phosphate glasses are widely used for photonics application because they possess good rare-earth (RE) ions solubility, without clustering effect, due to their more open and distorted network than silica-based glass (Sh,05).

2.2.2 Laser glasses

Laser glasses are optical materials that are doped with rare-earth (RE) elements, which include Scandium, Yttrium and the elements in the lanthanide series in the periodic table. RE ions are used to detect, convert, and amplify photonic signals.

In this work, Er^{3+} ions have been studied as a source of laser emission. Utilizing the 980 nm excitation wavelength of the laser diode, Er^{3+} is first excited to $^4I_{11/2}$ level (second excited level), followed by a non-radiative transmission to the $^4I_{13/2}$ level (first excited level) (Ga,06). Next, emission at near infrared (NIR) region, at wavelength of 1.54 μm (wavelength widely used in telecommunications), is achieved by the radiative transition from the $^4I_{13/2}$ level to the ground state $^4I_{15/2}$ (Ga,06). The excitation can also be achieved through other higher levels from which nonradiative decay occurs to the metastable $^4I_{13/2}$ level (Ya,00). The energy levels and transitions are presented in Figure 3.

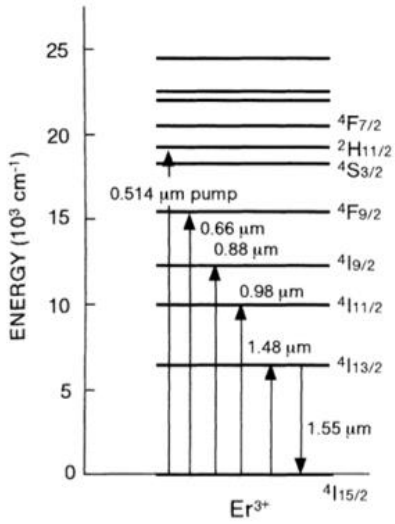

Figure 3. *Energy levels and transition wavelengths of Er_{3+} (Ya, 00).*

In laser glasses, photons excite the RE ions while the light passes through the glass. A traveling photon may stimulate the emission of another photon situated on an excited level. If emission happens, the emitted photon travels with the same phase and in the same direction, hence, contributing to the overall signal and amplifying it. The benefit of such a mechanism is efficiently utilized in fibers: amplified laser signal travels long distances with negligible losses.

2.3 Glass-Ceramics

2.3.1 Definition

Glass-ceramics (GCs) are materials formed through the controlled nucleation and crystallization of glass using heat treatment (Ho,12). These materials exhibit various physical, chemical, and optical properties, which is usually a combination of two or more desired properties in one material (Da,17).

Physically, glass-ceramics form an amorphous glass network in which crystals are homogeneously embedded. Crystalline phases may possess cleavage planes and grain boundaries acting as obstacles for fracture propagation, which is due to crystals having discrete structural plans and producing structural discontinuities if they meet (Ho,12). Thus, glass-ceramics are better in terms of mechanical properties than glasses.

Moreover, fluorine containing glass-ceramics doped with Er-ions are one of the most advantageous materials for spectroscopic applications (Ar,15). This is due to the fact that a nanocrystal incorporated with the Er_{3+}-ion possesses the low phonon energy needed for the successful upconversion(Ka,16).

2.3.2 Nucleation and growth theory

One of the methods to manufacture glass-ceramics is to induce internal crystallization through exposure of the glass to heat treatment. The process consists of two distinct stages: nucleation and crystal growth.

According to (Ho,12) classical definition, “a nucleus is an entity that already belongs to the new phase but is in an unstable equilibrium with respect to the supersaturated parent phase”. First, the nuclei are formed within the bulk, and then, the nuclei are grown into crystals. The visual representation of this process is depicted in Figure 4.

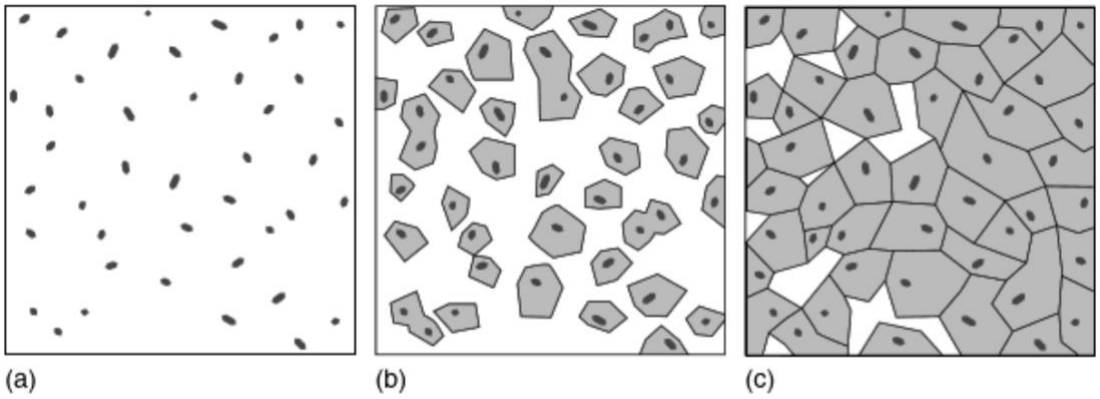

Figure 4. *Nucleation and growth mechanism: a) nuclei formation b) crystal growth of the nuclei c) glass-ceramic microstructure (Ho,12).*

To design a proper controlled heat treatment process, glass transition and crystallization temperatures should be defined. The Differential Thermal Analysis (DTA) is carried out on glass samples to establish their unique thermal properties.

Figure 5 (i) describes the rates of nucleation and crystal growth as a function of temperature.

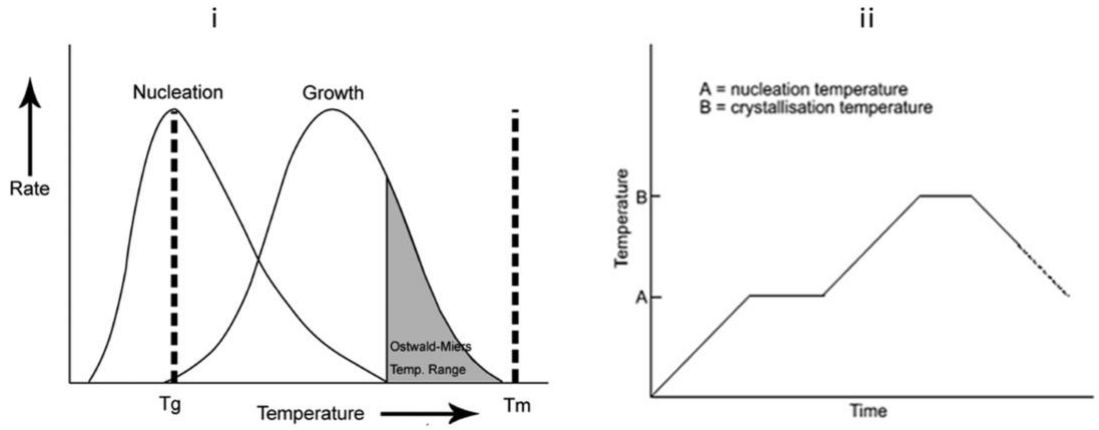

Figure 5. *(i) The rates of nucleation and crystal growth as a function of temperature. (ii) Two-step heat treatment for development of GCs. Modified from (Ka,14).*

One should point out that the width and temperature range of the nucleation and growth curves vary based on the glass composition. Typically, nucleation process is present at temperature range of T_g, and crystal growth occurs at higher temperatures (Ka,14). Only after the nuclei radius *r* is bigger or equal to this critical value, *r**, the crystal growth may start. At the Ostwald-Miers temperature range (metastable supercooling), the crystallization is initiable only if and from the nuclei developed in the nucleation temperature range (Ho,12).

Figure 5 (ii) illustrates the heat treatment process as a variation between the glass transition (nucleation) and crystallization temperatures. It is important to acknowledge that if a glass is cooled down from high temperature and if it is heat-treated in the Ostwald-Miers range, nucleation and growth cannot be induced, so, nuclei and crystals are not being formed.

As it was mentioned above, nucleation is the formation of crystal-like structures that are able to grow further. Homogeneous nucleation presumes the same probability of critical nucleus formation in any given volume of the glass, while heterogeneous nucleation occurs when incorporating nucleation sites to the glass (Ma,15).

The change in Gibbs-free energy ΔG is the bulk free energy change per mole on crystallization and is a thermodynamic driving force for the glass-crystal phase transition. The dependence between Gibbs free energy (ΔG) and radius of nuclei (r) is represented in the Figure 6.

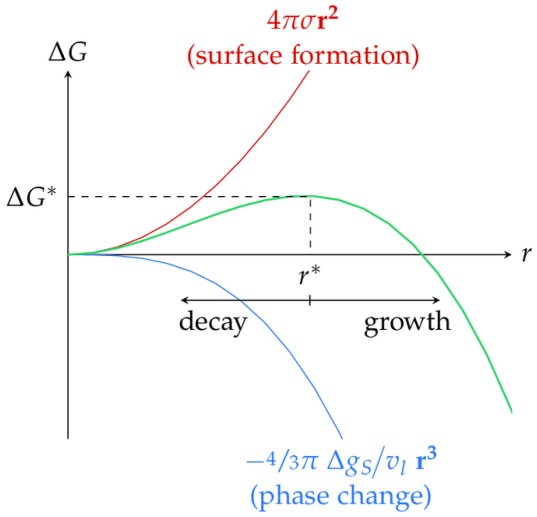

Figure 6. *Gibbs free energy (ΔG) as a function of the radius of nuclei (r) (He,15).*

The change in Gibbs free energy per mole is described by the following equation:

$$\Delta G = -\frac{4}{3}\pi r^3 \Delta g_v + 4\pi r^2 \gamma + \Delta G_E \quad (1)$$

Where nuclei radius is r, the interfacial energy that corresponds to the required energy for the formation of the new surface of the nucleus is γ, Δg_v is the free-energy change per unit volume that is produced by the formation of nuclei and ΔG_E is the fraction representing elastic distortion energy during a structural change (Ho,12).

When ΔG is negative, there exists an important prerequisite for the development of particles capable of growing. If a particular minimum size *r** (critical nucleus size) is achieved, the surface term ($4\pi r^2\gamma$) and the elastic strain term (ΔG_E) are smaller than the volume term ($-\frac{4}{3}\pi r^3 \Delta g_v$). The theoretical derivation of nuclei with the critical radius (*r**), without considering ΔG_E is as follow (Ho,12):

$$r^* = -\frac{2\gamma}{\Delta g_v} \quad (2)$$

Next, the kinetic barrier at which the change of free energy is sufficient for growing the nuclei into crystals (*ΔG**) is given by:

$$\Delta G^* = -\frac{16\pi\gamma^3}{3(\Delta g_v)^2} \quad (3)$$

Particles that achieved radius *r** or larger are capable of growing further and form crystals, whilst particles that did not achieve critical radius are called subcritical particles and are subject to disintegration in the glass (Ho,12).

2.3.3 Previous work on Er3+ doped glass-ceramics

In previous studies (No,18), (Sz,19), glasses within the system $75NaPO_3$–$(25-x)CaO$–$xCaF_2$–$0.15Er_2O_3$ (in mol%) with $x = 0$, 10, 20 and 25 were investigated. The study showed that bulk crystallization of CaF_2 doped with Er^{3+} occurred in the glass x=25 during heat treatment. However, such glass retains low thermal stability indicated by T_x-T_g~50°C, with T_x and T_g being the onset of the crystallization temperature and the glass transition temperature, respectively. Thus, this glass cannot be drawn into fiber.

This study will focus on improving the thermal stability of the glass while ensuring the preservation of the nucleation and growth mechanisms.

3. MATERIALS AND METHODS

3.1 Preparation of the samples

Glasses with the system (100-x-0.25)(75$NaPO_3$ – 25CaF_2) – xFe_2O_3 – 0.25Er_2O_3 with x = 0, 1.5, 2.5, 5, and 10 in mol% were prepared using standard melting procedure. The batches were prepared using the following chemicals: granular $(NaPO_3)_6$ from Alfa Aesar, 99.99% purity; mesh powder CaF_2 from Alfa Aesar, 99.95% metals basis; powder Er_2O_3 from Aldrich, 99% trace metals basis; powder Fe_2O_3 from Sigma-Aldrich, purity greater or equal to 99%. The batches were melted in a quartz crucible in air for 5 minutes at temperature range 950-1050°C, depending on the glass composition. Table 1 summarizes the melting temperature used to prepare the different glasses.

Table 1. *Melting temperatures of the glasses.*

Sample code	Melting temperature T_m (°C)
0Fe	950
1.5Fe	1050
2.5Fe	1050
5Fe	1050
10Fe	1050

The melting temperature has to be increased when melting the batches containing Fe_2O_3 in order to prepare a crystal-free material after quenching. After quenching, the glasses were annealed at 200°C for 5 hours to release the stress which appeared during the quenching process.

3.1.1 Glass-ceramics

Glass-ceramics were prepared employing the nucleation and growth theory from the as-prepared glasses. At first, the glasses were held at glass transition temperature T_g + 20°C for 17 hours to create the nuclei and then, to induce internal crystallization, the temperature was increased to the glass crystallization temperature (T_p) of each glass and maintained for 1 and 6 hours for each sample as performed in (No,18), (Sz,19).

3.2 Scanning Electron Microscope (SEM)

Surface topography and composition analysis of the glass samples were conducted using the Carl Zeiss Crossbeam 540 Gemini Scanning Electron Microscope (SEM) connected with an Oxford Instruments Energy Dispersive X-ray Spectroscopy (X-MaxN

80) detector (EDS). Before the analysis, the glass samples needed to be polished and coated with carbon. Generally, non-conductive samples are coated with carbon to enhance the image contrast. Polishing is required for obtaining flat surfaces without scratches, otherwise, the uneven sample profile will interfere the signal approaching the detector.

One of the main advantages of SEM over light microscope is the significantly improved resolution achieved by the fact that electrons possess smaller wavelengths than photons do. Using SEM, it is possible to scan and produce an image of very fine details. Figure 7 describes the schematic outline of a scanning electron microscope basis components.

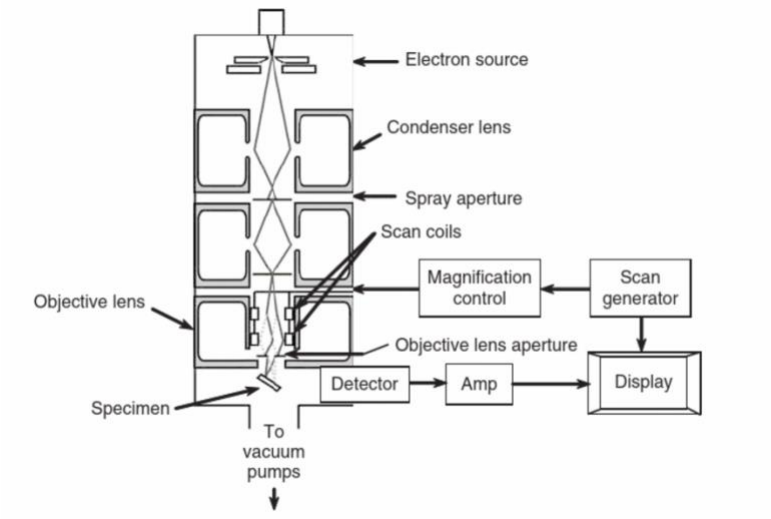

Figure 7. *Schematic diagram of SEM equipment (St,08).*

Primary electrons are generated in an electron source. They are accelerated and formed into a finely focused beam, which is modelled by a lens (or combination of lenses) and aperture. The location of the electron beam on the specimen is regulated using scan coils, which create a raster-like pattern rather than a spot. Finally, the objective lens controls the focus of the beam on the sample. (St,08)

When the beam reaches the sample and the primary electrons interact with the material, they produce various charged particles and photons are emitted back from the sample

surface. The examples of signals and irradiations generated in an electron-sample interaction are shown in Figure 8.

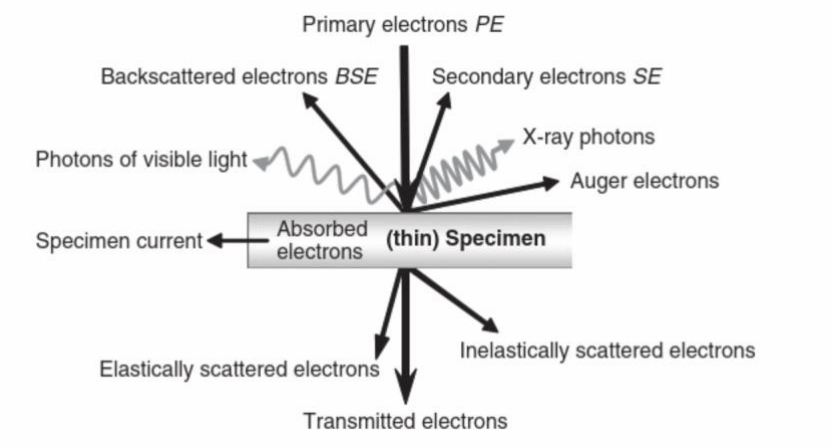

Figure 8. *Examples of useful signals produced when the electron beam strikes the sample (St,08).*

The generated signals may be collected to an image, diffraction pattern or chemical spectrum. The fundamental signals are backscattered electrons (BSE) and secondary electrons (SE); their generation, transport and escape are determined by different surface topography and chemical composition of the samples. The SEM image is formed accordingly, based on variations of the signals, by scanning the arbitrary area point by point. (St,08)

3.3 X-ray Diffraction (XRD)

The equipment was Panalytical EMPYREAN multipurpose X-Ray Diffractometer (XRD) with nickel filtered copper K-Alpha radiation. The spectra were acquired utilizing the Bragg-Brentano geometry and by rotating the sample holder around the Phi-axis at a constant speed of 16 revolutions per minute.

The XRD operation principle involves production of X-rays with typical wavelength of about 1_{-10} m, which is in range of the interatomic spacing in crystals. Elastic scattering happens when the X-rays hit the specimen. Generated scattered X-rays have the same wavelength as the incident, while different intensities and spatial distributions form a unique diffraction pattern defined by the exclusive composition and structure of the sample.

X-ray diffractometers may have different configurations based on the sample requirements; however, there are five common components in each system. The typical schematic representation of an X-ray diffractometer is depicted in Figure 9.

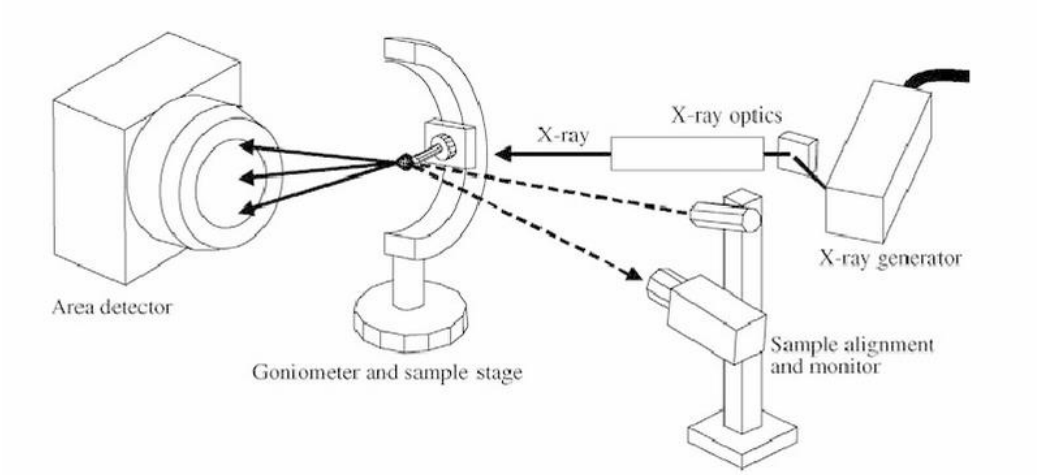

Figure 9. *The schematic representation of basic components in an X-ray diffractometer (He,09).*

X-ray generator produces primary X-rays, which are then processed by the X-ray optics to be at the required wavelength and meet other important parameters for the diffraction. Goniometer and sample stage rotate the sample to establish the necessary geometry to satisfy the Bragg's condition. Sample alignment and monitor are used for correct sample positioning in the machine and for monitoring its state. Finally, the area detector collects the scattered X-rays to produce a diffraction pattern.

The Bragg law is considered to be one of the fundamental ways to outline the principle of the X-rays diffraction. The required condition is described by the following equation:

$$n\lambda = 2d\sin\theta \qquad (4)$$

where n stands for the order of reflection and is an integer number, λ is the wavelength of the produced X-rays, d is the distance between each adjacent crystal planes, and θ is the Bragg angle at which the diffraction peak is observed (He,09).

Figure 10 illustrates the Bragg's condition in practice.

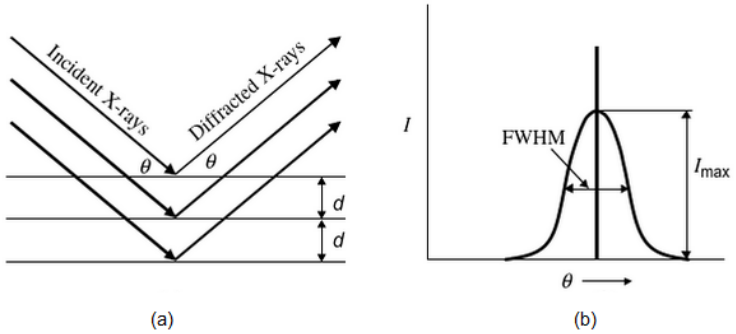

Figure 10. *The Bragg's condition illustrated (a). The diffraction peak for the angle θ (b) (He,09).*

In the picture, incident X-rays are hitting the surface at an angle θ, thus, producing diffracted X-rays with maximum intensity (diffraction peak).

3.4 Physical properties

The density of the glass samples was determined employing the Archimedes' principle which implicates that the force acting on the sample immersed in liquid is equal to the weight of the displaced liquid. This approach is convenient for the density measurements of the samples with irregular shape, which glass pieces have. Ethanol was chosen as the immersion liquid as the glasses are hygroscopic.

The measurement was conducted using an OHAUS Adventurer Analytical scale along with the density measurement kit. First, the weight of the sample in air and then in ethanol was measured. Second, the Equation 5 was used to calculate the density of glass:

$$\rho_{sample} = \rho_{liquid} \frac{m_{in\ air}}{m_{in\ air} - m_{in\ liquid}} \quad (5)$$

where $m_{in\ air}$ is the mass of the sample in air, $m_{in\ liquid}$ stands for the mass of the sample in the immersion liquid (ethanol), ρ_{sample} is the density of the sample, and ρ_{liquid} is the density of immersion liquid (ethanol) at the temperature at the time of measurements.

The accuracy of measurement is ±0.02g/cm3.

3.5 Thermal properties

The thermal analysis of the glass is performed in order to evaluate its characteristic temperatures, which include the glass transition temperature T_g, the onset of crystallization T_x, and the crystallization temperature T_p. The glass transition temperature is indicated by a discontinuous change in the specific heat of the material happening due to a glass converting from solid to the liquid state. Then, the increase in the specific heat of the material causes "a shift in the baseline, or offset, of the curve" indicating the onset of crystallization temperature. The next feature in the thermogram is the enthalpy being released from the glass as a corollary of crystallization and the glass structure becomes more ordered. Clearly, this point at the thermogram implies the crystallization temperature. (Sh,05)

The measurements were carried out using NETZSCH STA 449 F1 Differential Scanning Calorimetry (DSC) equipment with a heating rate of 10oC/min. The schematic of the equipment is depicted in Figure 11.

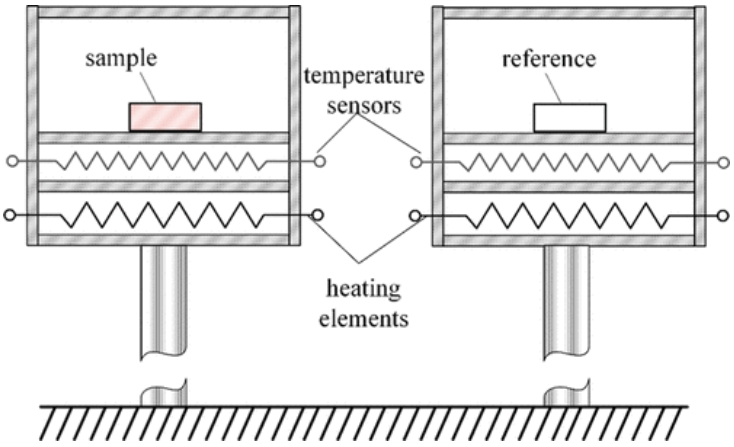

Figure 11. *Schematic representation of the DSC equipment (Zh,19).*

Measurement principle is as follows: powder glass sample on a platinum pan is placed in one microfurnace and an inert reference in the other. Both microfurnaces are heated at a controlled rate (10$_o$C/min) with the same electrical power supplied. If any thermal events such as glass transformation, crystallization or phase transformations occur take place on the investigated sample, a temperature difference between the sample and the reference is measured and, based on it, the heat flow of the sample is plotted as a function of temperature. (Zh,19)

The result of a DSC measurement is a DTA curve or a thermogram (shown in Figure 12). The direction of the curve points out the nature of the process: exothermic where the energy is released or endothermic where the energy is absorbed.

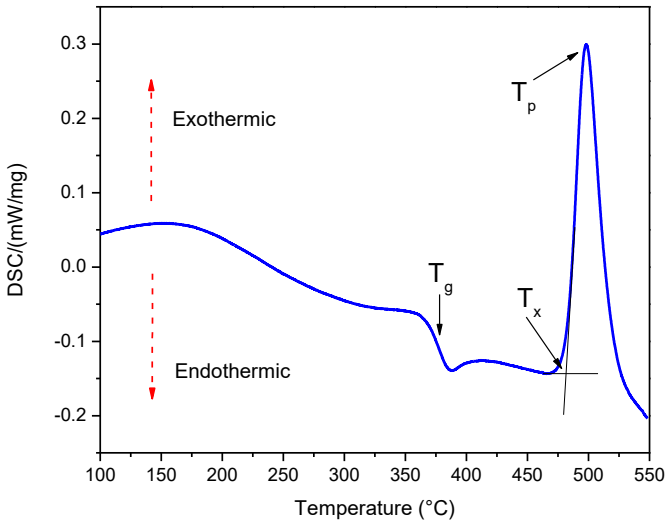

Figure 12. *Thermogram of the glass with x=5, taken as an example.*

The glass transition temperature T_g is evaluated at the inflection point of the endotherm, which can be found at the minimum of the first derivative of the DTA curve. The onset of crystallization T_x is the onset of the exothermic peak. The crystallization temperature T_p

is the maximum value of the exothermic peak. The accuracy of each temperature value is ±3°C.

3.6 Optical properties

In this study, the absorption spectra of the polished glass samples were measured using an UV-Vis-NIR spectrophotometer (UV-3600 Plus, Shimadzu). The range of the measurement was set to 200-1700 nm with a 0.5 nm interval. In order to determine the absorption coefficient and absorption cross-section, the thickness of the samples was measured with a digital caliper; measurements possess an accuracy of ± 0.05 mm.

Light interaction with the glass can be studied in terms of light absorption. Light absorption implies the material absorbing photons, which have the equivalent energy to an electronic transition to a higher state. Thus, when the light is passing through the sample, its intensity decreases because of the lowered number of photons.

A spectrometer is used to measure the light intensity as a function of wavelength. In absorption measurement, the wavelength of the light travelling through the sample is varying and by measuring the intensity of the particular outcoming wavelength, an absorption spectrum is produced. A schematic of a spectrophotometer is depicted in Figure 13.

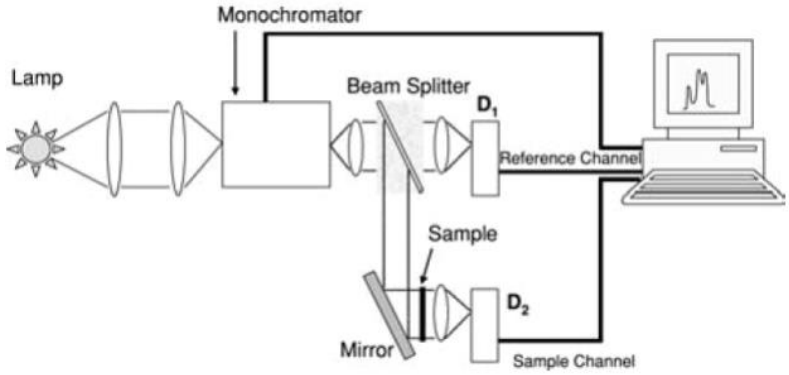

Figure 13. *Schematic diagram of a spectrometer (So,05).*

In a spectrometer, the monochromatic beam of light is produced by the monochromator, after which the beam is split into two identical beams. One of the beams is passed through the sample and the other one goes uninterrupted. As a result, the detector measures two intensities I_0 and I, the reference intensity and intensity altered by the sample's absorption respectively. (So,05)

The absorbance A evaluates to what extent the light is absorbed and is calculated by taking the ratio of the two above mentioned intensity values according to the following formula:

$$A = \log\left(\frac{I}{I_0}\right) \tag{6}$$

The absorption coefficient (cm^{-1}) takes into account the thickness of the samples and is calculated with the Beer Lambert-law:

$$\alpha = \frac{\ln(10)}{L} A \quad (7)$$

where L is the thickness of the sample in cm. (So, 05)

Next, the absorption cross-section $\sigma(\lambda)$ (cm^2), which provides the information about absorption taking into account the number of absorbing particles, is calculated using the following equation:

$$\sigma = \frac{\ln(10)}{NL} A \quad (8)$$

where N is the RE-ion concentration ($ions/cm^3$) calculated from RE-ion mol% and the density of a glass.

The absorption coefficient possesses an accuracy of ± 10%.

3.7 Structural analysis

The IR spectra of the glasses crushed into powder were measured using a Perkin Elmer Spectrum FTIR2000 using Attenuated Total Reflection (ATR) mode in the range of 650–1600 cm^{-1}. The resolution of the measurement was 2 cm^{-1} and the spectra were obtained from the accumulation of 8 scans.

Infrared (IR) region covers a range of frequencies in an electromagnetic spectrum, which is commonly defined in between 14300 and 20 cm^{-1}. By exposing a sample to IR radiation, changes in the vibrational energy levels and dipole moment of molecules are observed. These characteristics depend on the strength of the chemical bond between atoms and the mass of each atom. Therefore, the spectrum of the radiation collected after the incident IR-beam passed through the sample provides the information about the structure of the studied sample. (Mo,16)

The Fourier-transform infrared spectroscopy (FTIR) technique is used for this measurement. Figure 14 depicts a schematic representation of a typical Fourier Transform Infrared Spectrometer setup.

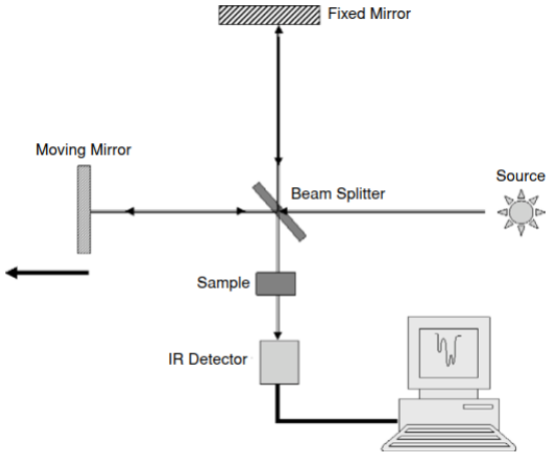

Figure 14. *Schematic diagram of an FTIR spectrometer. (So,05)*

The setup employs a Michelson interferometer with a beam splitter, which divides the incident IR radiation into two beams; one directed to the fixed mirror and the other one to the moving mirror. The beams recombine at the beam splitter after being reflected from the mirrors. They may produce constructive or destructive interference based on the path differences. Then, the IR radiation travels through the sample located between the beam splitter and detector. An interferogram of a IR-spectrum in frequency domain is produced after the Fourier transform of the fluctuations in intensity of the measured IR-radiation obtained in time domain. (Re,10)

Additionally, the Attenuated Total Reflectance (ATR) technique was used in this study. The schematic of an ATR is presented in Figure 15.

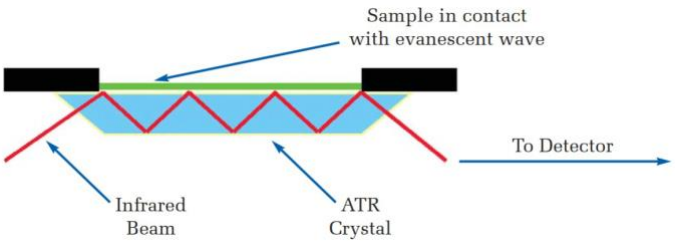

Figure 15. *Schematic diagram of the ATR setup. (ATR,05)*

The operation principle is as follows: sample should be in direct contact with the ATR crystal, which must have a considerably larger refractive index than that of the sample since the internal reflectance is required. The infrared beam undergoes a total internal reflection while travelling between the surfaces. This produces the evanescent wave, which extends beyond the crystal penetrating the sample, being absorbed. The absorption of the evanescent wave is then measured and an infrared spectrum of a studied sample is obtained. (Re,10)

3.8 Spectroscopic properties

The emission spectra of the glasses crushed into powder were measured in the range 1400-1700 nm with a 0.5 nm interval using a Jobin Yvon iHR320 spectrometer with a

Hamamatsu P4631-02 detector and a Thorlabs FEL 1500–filter. The excitation wavelength ~980 nm was provided with a monochromatic single-mode fiber pigtailed laser diode (CM962UF76P-10R, Oclaro). For these measurements, fine powder of each glass sample was placed in a sample holder at the room temperature to be able to compare the intensity of the emission between the samples.

An atomic system can be excited to a higher energy state from the ground state by a photon via collision. When the atom possesses an excited state, a spontaneous emission may occur and a new photon will be released, while the atom transitions to a lower energy state. Emitted photons have a specific wavelength based on the energy difference between the transition states of the system.

The emission spectroscopy utilizes the photoelectric effect as follows: the studied atomic system is bombarded with photons in order to excite the electrons, after which the wavelengths of the emitted photons are determined. The output of the measurement is an emission spectrum. Thus, the elemental composition of the studied sample can be analyzed. The emission principle for Er^{3+}-ions, emitting at 1.5 μm, was described in section 2.2.2.

The emission spectra can be obtained using an optical instrument called spectrofluorometer (So, 05). A schematic representation of a spectrofluorometer setup is shown in Figure 16.

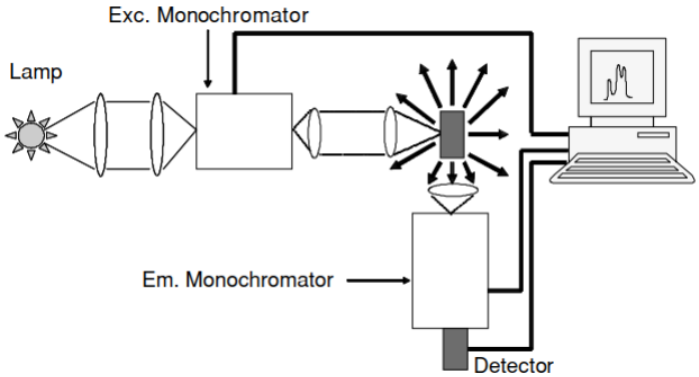

Figure 16. *Schematic diagram of a spectrofluorometer. (So,05)*

The excitation is achieved by using a light source and an excitation (Exc.) monochromator, which produces a light beam of a specific wavelength λ_{exc}. After excitation, the beam of emitted photons is collected by a focusing lens, after which the beam passes through the emission (Em.) monochromator and only a certain narrow spectral band travels to the detector, which measures the intensity of the band. Thus, the detector measures the intensities of the emission scanning through different wavelengths and an emission spectrum is constructed.

4. RESULTS AND DISCUSSION

Phosphate glasses have been of a great interest for research due to their low melting temperature, high electrical conductivity, high thermal expansion coefficients, and other physical properties. In (No,18), (Sz,19), bulk crystallization of CaF_2 doped with Er^{3+} was found to occur in the glass ($75NaPO_3$-$25CaF_2$) upon heat treatment leading to a strong increase in the intensity of the upconversion. However, the glass is a poor glass former (as evidenced by T_x-T_g~50°C) and so it cannot be drawn into fiber.

In this work, iron(III) oxide (Fe_2O_3) was added into the composition to order to increase the thermal stability of the original glass without changing the nucleation and growth mechanism. First, the impact of the addition of Fe_2O_3 on the physical, thermal, optical, structural and luminescence properties of the glass is reported. Then, we report the changes in those properties after heat treatment of the glasses.

4.1 Impact of the glass composition on various glass properties

Glass samples with the composition $(100\text{-}x\text{-}0.25)(75NaPO_3–25CaF_2)–xFe_2O_3–0.25Er_2O_3$ with x = 0, 1.5, 2.5, 5, and 10 in mol% were prepared using standard melting procedure. Melting temperature (T_m) of the samples containing iron was higher to ensure full melting of the batch. As compared to previous study (No,18), all the glasses were melted in quartz crucibles to avoid reaction between Fe (iron) and Pt (platinum).

Table 2 summarizes the thermal properties of the as-prepared glasses along with melting temperatures, and densities.

Table 2. *Melting temperatures, densities, and thermal properties of the as-prepared glasses.*

Sample code	Melting temperature T_m (°C)	Glass density ρ ± 0.02 (g/cm^3)	T_g ± 3 (°C)	T_x ± 3 (°C)	T_p ± 3 (°C)	ΔT= T_x-T_p ± 6 (°C)
x=0	950	2,67	338	425	457	87
x=1.5	1050	2,70	353	440	461	88
x=2.5	1050	2,72	359	469	490	110
x=5	1050	2,76	378	482	498	104
x=10	1050	2,85	401	522	549	121

With an increase in x, the density of the glass increases. This result is observed because the concentration of heavier element Fe is increasing. An increase in x also increases the glass transition temperature T_g, the onset of crystallization T_x, and of the maximum of the crystallization peak T_p. The values of ΔT indicating the thermal stability also increased.

Thermal stability of the glass parametrizes glass' kinetic resistance to the crystallization and needs to be about 100°C (preferably larger) to consider the glass a stable glass (Ce,11). Therefore, we show here that the addition Fe_2O_3 improves the thermal stability of the glass. Surprisingly, the ΔT of the glass with x=0 is larger than the one reported in (No,18). One should remind that the glasses have the same composition but they were prepared in different crucible (quartz and Pt crucibles).

The IR spectra of the investigated glasses, normalized to the band at 890cm^{-1}, are presented in Figure 17.

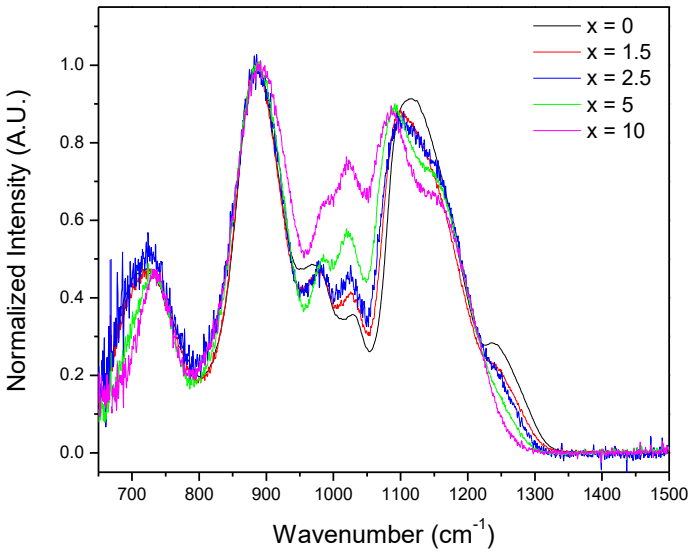

Figure 17. *Normalized IR spectra of the as-prepared glasses.*

The spectra exhibit bands at ~730 cm^{-1}, 890 cm^{-1}, 1020 cm^{-1} and 1090-1115 cm^{-1} and multiple shoulders in the range of 950-1000 cm^{-1}, 1130-1170 cm^{-1}, and 1220-1315 cm^{-1}. The bands at ~730 and 1080 cm^{-1} are assigned to symmetric stretching vibrations of (P-O-P) linkages connecting Q_2 units, while the 890 cm^{-1} band attributes the asymmetric stretching modes $(P\text{-}O\text{-}P)_{as}$ (Ve,13). The band at 1260 cm^{-1} can be related to asymmetric stretching modes $(O\text{-}P\text{-}O)_{as}$ fundamental vibrations of Q_2 units (Ko,10). The bands at 870, ~960 and ~1020 cm^{-1} can be assigned to the asymmetric stretching vibrations of Q_2 units in chains, small and large rings respectively (Ga,04). The shoulder at ~980 cm^{-1} and the band at 1085 cm^{-1} are related to the symmetric and asymmetric stretching vibration of PO_3^{2-} in Q_1 units, respectively (Ab,09). The Q_2 and Q_1 groups can also contribute to the bands at 1085 and 1190 cm^{-1} respectively.

An increase in *x* leads to a decrease in intensity of the bands at 730, 1090 and 1260 cm^{-1} and to an increase in intensity of the bands in the 950-1050cm^{-1} range indicating an increase in the Q_1 units at the expense of Q_2 units.

The absorption spectra of the as prepared glasses are presented in Figure 18.

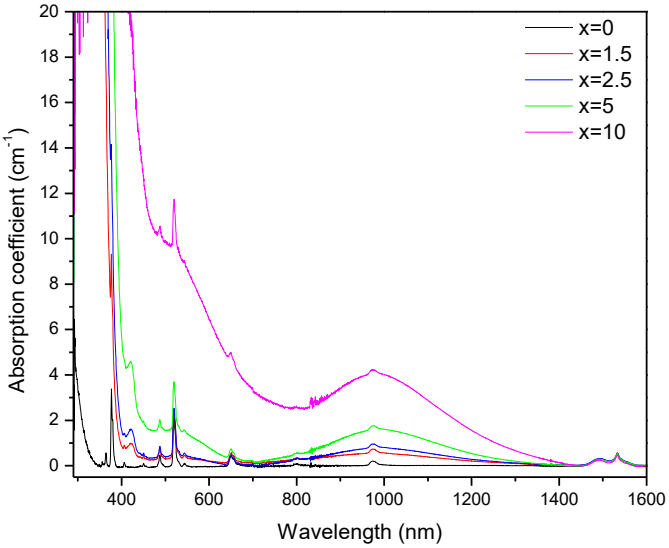

Figure 18. *Absorption spectra of the as-prepared glasses.*

The spectra exhibit bands in the visible which can be related to the Er^{3+} ion 4f- 4f transition from the ground state $^4I_{15/2}$ to various excited levels of Er^{3+} ions (Hr,17). An increase in x leads to a few modifications in the spectra: shift of the band gap to longer wavelength and appearance of the new bands at ~520 nm and ~980 nm. The appearance of the new bands can be attributed to Fe^{3+} and Fe^{2+} ions respectively, according to (Ch,05).

The absorption coefficients and cross-sections are listed in Table 3.

Table 3. *Concentration of Er^{3+} ions and absorption cross-sections of the as-prepared glasses.*

x	α_{Abs} at 980nm(cm^{-1})	α_{Abs} at 1532nm(cm^{-1})	Er^{3+} ions/cm^3 (10^{19}) ± 5%	σ_{Abs} at 980 nm (10^{-20}) cm^{-2} ± 10%	σ_{Abs} at 1532 nm (10^{-21}) cm^{-2} ± 10%
0	0.1867	0.5477	8.30	2.22	7.18
1.5	0.7178	0.5545	8.39	8.56	6.79
2.5	0.9397	0.5671	8.45	1.11	6.52
5	1.7527	0.5425	8.55	2.05	6.19
10	4.2105	0.4687	8.78	4.79	5.46

A significant increase in the absorption cross-section at 980 nm along with a slight decrease at 1532 nm can be observed as x increases. An increase at 980 nm can be associated to the presence of Fe^{2+}.

The emission spectra of the as-prepared glasses pumped with an excitation at 980 nm are presented in Figure 19.

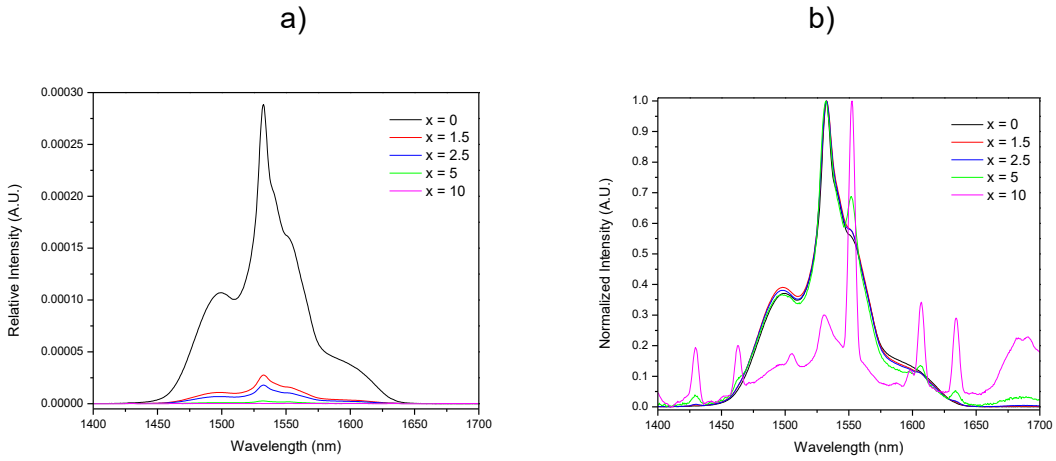

Figure 19. *Emission spectra (a) and normalized emission band (b) of the as-prepared glasses (λ_{exc}= 980nm).*

The spectra (except the glass with x=10) exhibit a typical emission broad band of Er^{3+} corresponding to a transition from the excited state $^4I_{13/2}$ to the ground state $^4I_{15/2}$ (No,18). The broad band indicates that the Er-ions are located in an amorphous site. The peaks seen in the emission band from the glass with x=10 clearly indicate that the glass is not amorphous. The melting temperature of this glass was probably too small leading to the fabrication of a partially crystallized glass.

With increase in x, a large decrease in intensity of the emission is observed. As the absorption coefficient at 980 nm increases, there, thus, might be an energy transfer to the Fe^{2+} ions.

As seen in Figure 18b, the shape of the band does not experience any significant changes when adding Fe_2O_3 in the glass, which implies that Er-ions are located in a similar site in all the glasses with x<10. Therefore, Fe ions are not suspected to enter in the first coordination shell of Er-ions.

4.2 Er^{3+} doped glass-ceramics

As in (No,18), the as-prepared glasses were heat treated at T_g + 20 °C for 17 hours followed by T_p for 1 and 6 hours in order to create glass-ceramics. The pictures of the as-prepared and heat treated glasses are shown in Figure 20.

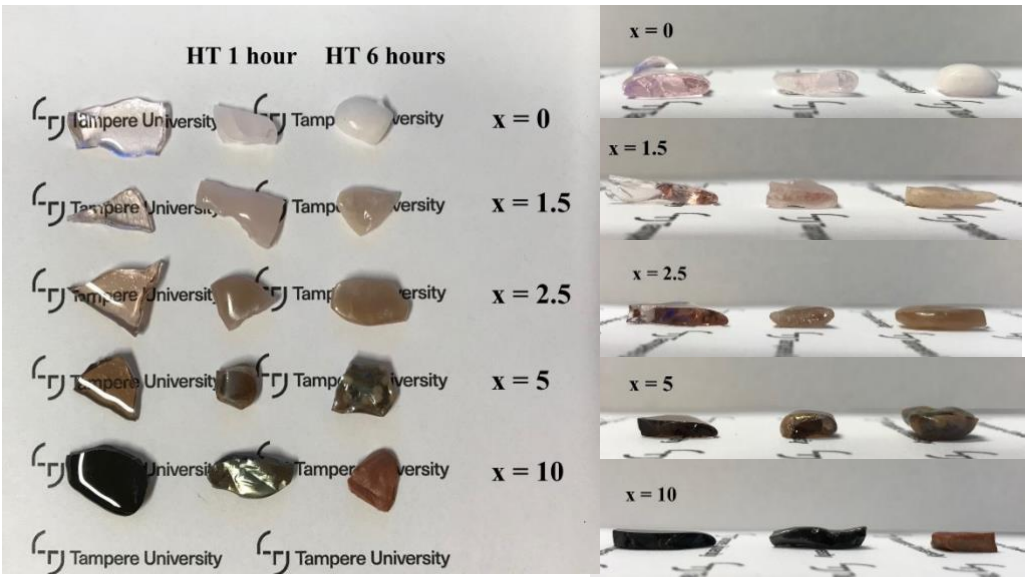

Figure 20. *Pictures of the as-prepared glasses prior and after the heat treatment for 1 and 6 hours.*

Surprisingly, the glass with x=0 becomes opaque after heat treatment and exhibit surface crystallization while transparent glass-ceramics were reported in (No,18), (Sz,19). As explained in (No,18), a decrease in CaF_2 content changes the crystallization tendency of the glass: glasses with low CaF_2 content were also opaque after heat treatment. Therefore, we suspect the glasses to contain a lower amount of CaF_2 than expected. All glasses, independently of x, exhibit surface crystallization.

The SEM images were collected in order to evaluate the crystals formed in heat-treated glass. SEM images of glasses with x=0, 1.5 and 10 heat treated for 6h, taken as an example, are presented in Figure 21.

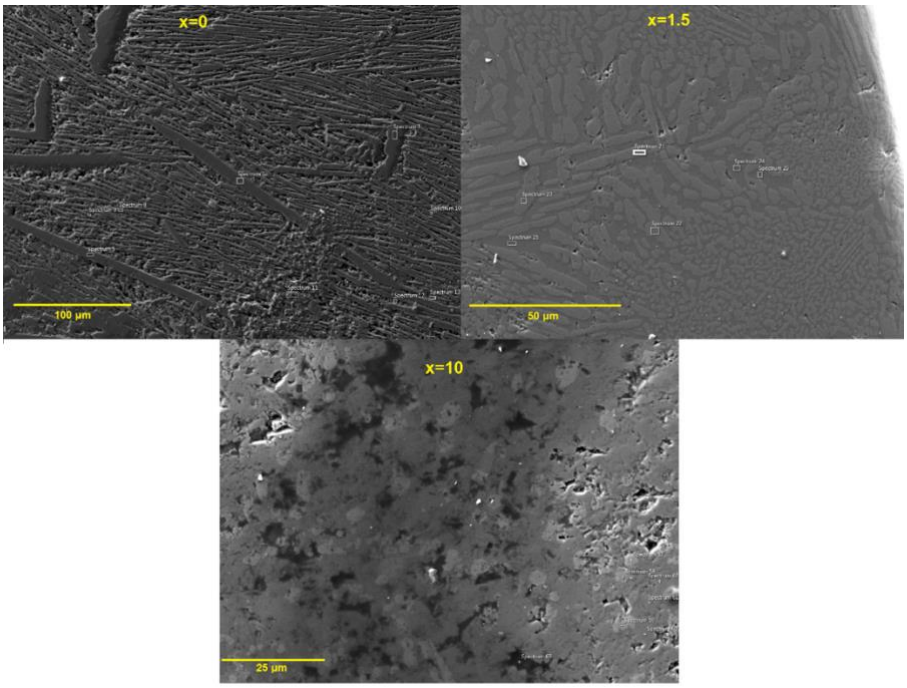

Figure 21. *SEM images of x=0, x=1.5 and x=10 samples (6 hours of HT).*

The SEM analysis confirmed surface crystallization of the glass. As seen in Figure 21, crystals with different shapes were found in the glasses while the CaF2 crystals were reported to have a round shape (No,18). In sample x=0, the crystals are more defined and sharp. In sample x=1.5, the crystals seem to be more round and shorter in general. In sample x=10, there are no prolonged and sharp crystals.

The XRD patterns of the glasses are presented in Figure 21.

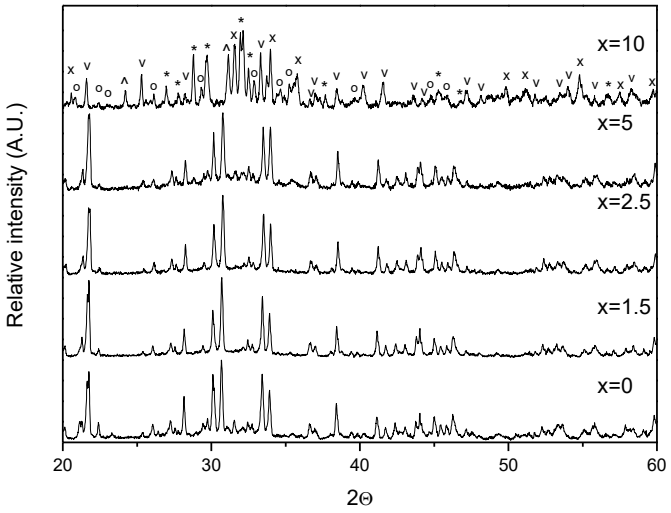

Figure 22. *XRD of the as-prepared glasses after the heat treatment for 6 hours. The crystals correspond to the symbols as following: $CaNaO_4P$ – v, $NaFeO_2$ – x, $Na_2Ca_2P_2O_7F_{20}$ – ^, $Ca_2P_2O_7$ – *, $NaPO_3$ – o.*

The XRD patterns exhibit different peaks which can be related to different crystals, the composition of which depends on the glass composition. Surprisingly, the glass with x=0 does not exhibit the peaks related to CaF_2 crystals but exhibits peaks which can be assigned to $NaPO_3$, $CaNaO_4P$, $Na_2Ca_2P_2O_7F_{20}$ and $Ca_2P_2O_7$. Similar crystals were found to precipitate in the glass with the composition (75 NaPO3-(25-x) CaO-xCaF2) with x between 10 and 20 mol%. Therefore, the glass with x=0 is confirmed to be less concentrated in F. As recently reported (Sz,19), the loss in F can be related to the use of Quartz crucible: SiF_4 is expect to form between CaF_2 and SiO_2 during the glass preparation as suggested in (Za,94). The decrease in the Fluorine content due to the use of quartz crucible is in agreement with the large ΔT measured for this glass as compared to the ΔT reported in (No,18) and also in agreement with the surface crystallization upon heat treatment.

An increase in x leads to a decrease in intensity of the peaks related to $Na_2Ca_2P_2O_7F_{20}$, $NaPO_3$ and to an increase of the peaks related to $Ca_2P_2O_7$. New peaks appear which can be related to $NaFeO_2$.

The emission properties of the heat treated glasses are presented in Figure 22 (next page). The heat treatment leads to a slight increase in the intensity of the emission except for the glass with x=0. The increase in intensity is stronger as x increases

indicating that an addition in Fe_2O_3 increases the crystallization tendency of the glass probably as it depolymerizes the glass network as discussed earlier.

One can also notice that the shape of the emission band changes after heat treatment: the emission band becomes narrower after heat treatment indicating that the heat treatment leads to changes in the site of the Er-ions. We think that the heat treatment reduces the site distribution of Er-ions as the band is narrower after heat treatment without exhibiting sharp peaks. Er ions are suspected to remain in the amorphous glass. It is interesting to point out that the emission band of Er in the glass with x=10 becomes broader after heat treatment indicating that the Er-ions are located in amorphous site after heat treatment.

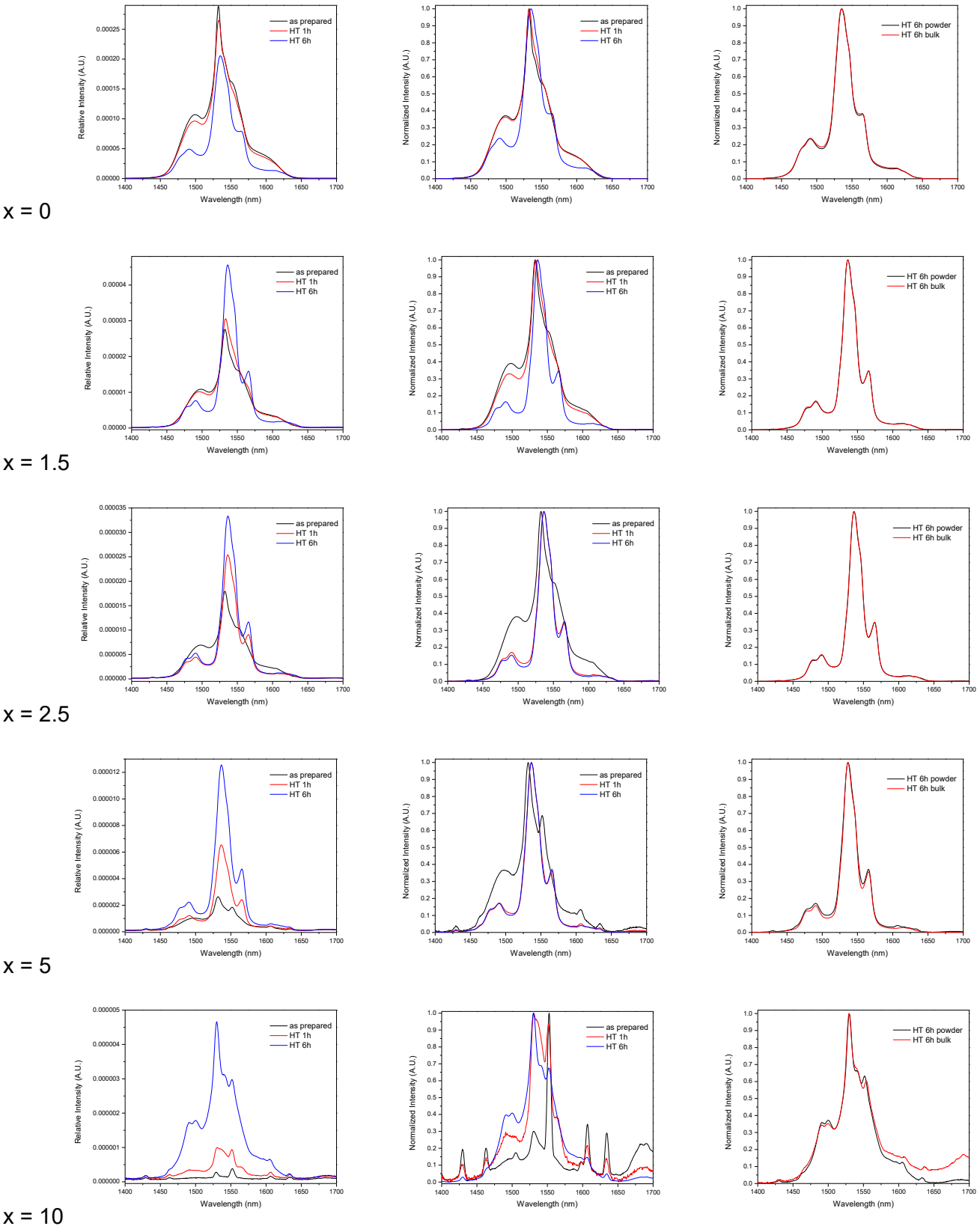

Figure 23. *Emission spectra (1st column), normalized emission band (2nd and 3d column) of the heat-treated glasses (λ_{exc} = 980nm).*

5. CONCLUSIONS

New glasses within the composition of (100-x-0.25)(75$NaPO_3$–25CaF_2)–xFe_2O_3–0.25Er_2O_3 with x = 0, 1.5, 2.5, 5, and 10 in mol% were prepared and characterized.

Density measurements and differential thermal analysis (DTA) were performed in order to study the effect of Fe_2O_3 addition on the physical and thermal properties of the new glasses. An increase in Fe_2O_3 concentration leads to an increase in the glass density due to an increase in the concentration of heavier element such as Fe. DTA revealed an increase in glass transition and crystallization temperatures, also showing an increase in ΔT, confirming that the new glasses are thermally stable and, therefore, can be drawn into fibers. From the structural analysis (IR spectroscopy), an increase in x leads to an increase in the Q_1 units at the expense of Q_2 units. In the absorption spectra of the glass, the addition of Fe_2O_3 leads to the appearance of new absorption bands which can be related to Fe^{2+} and Fe^{3+}. A significant decrease in intensity of the emission at 1.5 μm along with an increase in the absorption cross-section at 980 nm was observed and was associated with the energy transfer to the Fe^{2+} ions. The shape of the emission band did not experience any big changes with increase in x, except for the glass with x=10 indicating that in the as-prepared glasses Er-ions are located in the amorphous site of the glass free of Fe ions. The as-prepared sample with x=10 is most likely crystallized.

The as-prepared glasses were heat treated at T_g + 20 °C for 17 hours followed by T_p for 1 and 6 hours. The heat treatment changes the transparency of the glasses to opaque and led to surface crystallization, independently of x. An addition in Fe_2O_3 increases the crystallization tendency of the glass as it depolymerizes the glass network. Based on the previous study (No,18), the surface crystallization of the glass with x=0 was related to lower CaF_2 content than expected due to the use of quartz crucible for the melting of the glass. The surface crystallization was confirmed using SEM and XRD. The heat treatment led to surface crystallization with multiple crystals ($CaNaO_4P$, $NaFeO_2$, $Na_2Ca_2P_2O_7F_{20}$, $Ca_2P_2O_7$, $NaPO_3$) but no CaF_2 was detected in the glasses. As the concentration of Fe_2O_3 increases, the increase in intensity of the emission of the glass-ceramics compared to the as-prepared becomes stronger. From the shape of the emission band, Er-ions are suspected to remain in the amorphous glass.

This thesis was aimed to create and characterize new Er-doped glass-ceramics. The newly produced glasses proved to be thermally stable, which was the objective of this study. However, the impact of Fe_2O_3 addition on nucleation and growth mechanism was not studied “properly” because of losses of CaF_2 during the melting, which is due to use of quartz crucible. The study should be repeated using alumina crucible to avoid the losses of F during the glass melting.

REFERENCES

(Ab,09) Abou, E. N., Chrzanowski, W., Pickup, D. M., O'Dell, L. A., Mordan, N. J., Newport,... R. J., Knowles, J. C. (2009). Structure and properties of strontium-doped phosphate-based glasses. Journal of the Royal Society Interface, 6(34), 435-446. doi:10.1098/rsif.2008.0348

(Ar,15) Aroda, M., Szlosarczyk, K., RoA1, Sitarz, M., & JeleA, P. (2015). Spectroscopic properties of transparent er-doped oxyfluoride glass-ceramics with GdF.sub.3. Spectrochimica Acta Part A: Molecular and Biomolecular Spectroscopy, 134, 631. doi:10.1016/j.saa.2014.06.066

(ATR,05) FT-IR Spectroscopy Attenuated Total Reflectance (ATR) (2005). Perkin Elmer Life and Analytical Sciences.

(Br,00) Brow, R. K. (2000). Review: The structure of simple phosphate glasses doi://doi-org.libproxy.tuni.fi/10.1016/S0022-3093(99)00620-1

(Ce,11) Çelikbilek, M., Ersundu, A. E., Solak, N., & Aydin, S. (2011). Investigation on thermal and microstructural characterization of the TeO2–WO3 system doi://doi.org/10.1016/j.jallcom.2011.02.109

(Ch,05) Chakradhar, R., Ramesh, K. P., Rao, J. L., & Ramakrishna, J. (2005). The effect of mixed alkali on EPR and optical absorption spectra in mixed alkali borate xNa(2)O-(30-x)K2O-70B(2)O(3) glasses doped with iron ions. Journal of Non-Crystalline Solids, 351(14-15), 1289-1299. doi:10.1016/j.jnoncrysol.2005.03.001

(Da,17) Davis, M., & Zanotto, E. (2017). Glass-ceramics and realization of the unobtainable: Property combinations that push the envelope. MRS Bulletin, 42(3), 195-199. doi:10.1557/mrs.2017.27

(De,98) Dejneka, M. J. (1998). Transparent oxyfluoride glass ceramics. MRS Bulletin, 23(11), 57-62.

(Ga,04) Gao, H., Tan, T., & Wang, D. (2004). Effect of composition on the release kinetics of phosphate controlled release glasses in aqueous medium. Journal of Controlled Release, 96(1), 21-28. doi:10.1016/j.jconrel.2003.12.030

(Ga,06) Gan, F., & Xu, L. (2006). Photonic glasses. Singapore: World Scientific Publishing Co Pte Ltd.

(Gl,19) Glass. (2019). In Encyclopædia Britannica. Retrieved from https://academic-eb-com.libproxy.tuni.fi/levels/collegiate/article/glass/36988

(He,09) He, B. B. (2009). Two-dimensional x-ray diffraction , John Wiley & Sons, Incorporated, pp. 13-25.

(He,15) Heinze, David. (2015). Physically-based models for two-phase flow phenomena in steam injectors: a one-dimensional simulation approach. doi:10.5445/KSP/1000048586.

(Ho,12) Holand, W., & Beall, G. H. (2012). Glass ceramic technology. Somerset: John Wiley & Sons, Incorporated.

(Hr,17) Hraiech, S., Bouzidi, C., & Férid, M. (2017). Luminescence properties of Er3+-doped phosphate glasses doi://doi-org.libproxy.tuni.fi/10.1016/j.physb.2017.07.047

(Ka,16) Kang, L., Song, X. Q., Huang, X. J., Qiu, J. R., & Dong, G. P. (2016). Enhanced emission and spectroscopic properties in oxyfluoride glass ceramics containing LaOF: ER3+ nanocrystals. Optical Materials Express, 6(7), 2351-2359. doi:10.1364/OME.6.002351

(Ka,14) Karpukhina, N., Hill, R. G., & Law, R. V. (2014). Crystallisation in oxide glasses - a tutorial review. Chemical Society Reviews, 43(7), 2174-2186. doi:10.1039/c3cs60305a

(Kh,15) Khayyami, A. (2015). Low temperature sol-gel on polymeric substrate: Master of science thesis. Tampere: Tampere University of Technology.

(Ko,10) Konidakis, I., Varsamis, C.E., Kamitsos, E.I., Mo¨ncke, D. & Ehrt, D. (2010). Structure and properties of mixed strontium–manganese metaphosphate glasses, The Journal of Physical Chemistry C, Vol. 114(19), pp. 9125-9138. doi:10.1021/jp101750

(Le,14) Le Bourhis, E. (2014). Glass: Mechanics and technology (Second ed.). Weinheim, Germany: Wiley-VCH.

(Ma,15) Marghussian, V. (2015). Nano-glass ceramics : Processing, properties and applications. Norwich: Elsevier Science & Technology Books.

(Mo,15) Mogus-Milankovic, A., Santic, A., Pavic, L., & Sklepic, K. (2015). Iron phosphate glass-ceramics. Croatica Chemica Acta, 88(4), 1-8. doi:http://dx.doi.org/10.5562/cca2759

(Mo,16) Moore, E. (2016). Fourier transform infrared spectroscopy (FTIR): Methods, analysis, and research insights. Hauppauge, New York: Nova Science Publishers, Inc.

(No,18) Nommeots-Nomm, A., Boetti, N. G., Salminen, T., Massera, J., Hokka, M., & Petit, L. (2018). Luminescence of Er3+ doped oxyfluoride phosphate glasses and glass-ceramics doi://doi-org.libproxy.tuni.fi/10.1016/j.jallcom.2018.04.101

(Re,10) Rees, O. J. (2010). Fourier transform infrared spectroscopy : Developments, techniques, and applications. New York: Nova Science Publishers, Inc.

(Sh,05) Shelby, J. E. (2005). Introduction to glass science and technology (2nd ed.). Cambridge: Royal Society of Chemistry.

(So, 05) J.G. Sole´, L.e. Bausa´, D. Jaque (2005). Fundamentals, An Introduction to the Optical Spectroscopy of Inorganic Solids, John Wiley & Sons, Ltd.

(St,08) Stokes, D. (2008). Principles and practice of variable pressure/environmental scanning electron microscopy (vp-esem) : Environmental scanning electron microscopy (vp-esem).

(Sz,19) Szczodra, A., Kuusela, L., Norrbo, I., Mardoukhi, A., Hokka, M., Lastusaari, M., & Petit, L. (2019). Successful preparation of fluorine containing glasses with persistent luminescence using the direct doping method. Journal of Alloys and Compounds, 787, 1260-1264. doi:10.1016/j.jallcom.2019.02.075

(Ve,13) Vedeanu, N., Cozar, O., Stanescu, R., Cozar, I. B., & Ardelean, I. (2013). Structural investigation of new vanadium–bismuth–phosphate glasses by IR and ESR spectroscopy doi://doi.org/10.1016/j.molstruc.2013.01.078

(We,19) Wenzel, J. (2019). Glass. In AccessScience. McGraw-Hill Education. doi://doi-org.libproxy.tuni.fi/10.1036/1097-8542.290700

(Xu,06) Xu, L., & Gan, F. (2006). Photonic glasses. New Jersey: World Scientific.

(Ya,00) Yamane, M., & Asahara, Y. (2000). Glasses for photonics. Cambridge: Cambridge University Press.

(Za,94) Zaitsev, A. I., Leites, A. V., Litvina, A. D., & Mogutnov, B. M. (1994). Investigation of the mould powder volatiles during continuous casting. Steel Research, 65(9), 368-374. doi:10.1002/srin.199401179

(Za,17) Zanotto, E. D., & Mauro, J. C. (2017). The glassy state of matter: Its definition and ultimate fate doi://doi-org.libproxy.tuni.fi/10.1016/j.jnoncrysol.2017.05.019

(Zh,19) Zheng, Q. J., Zhang, Y. F., Montazerian, M., Gulbiten, O., Mauro, J. C., Zanotto, E. D., & Yue, Y. Z. (2019). Understanding glass through differential scanning calorimetry. Chemical Reviews, 119(13), 7848-7939. doi:10.1021/acs.chemrev.8b00510